UAVLight: A Benchmark for Illumination-Robust 3D Reconstruction in Unmanned Aerial Vehicle (UAV) Scenes

Kang Du[1,4]   Xue Liao[1,4]   Junpeng Xia[4]   Chaozheng Guo[4]   Yi Gu[1]   Yirui Guan[3]
Duotun Wang[1]   ShengHuang[4]   Zeyu Wang[1,2*]

[1]The Hong Kong University of Science and Technology (Guangzhou)
[2]The Hong Kong University of Science and Technology
[3]Beijing University of Chemical Technology
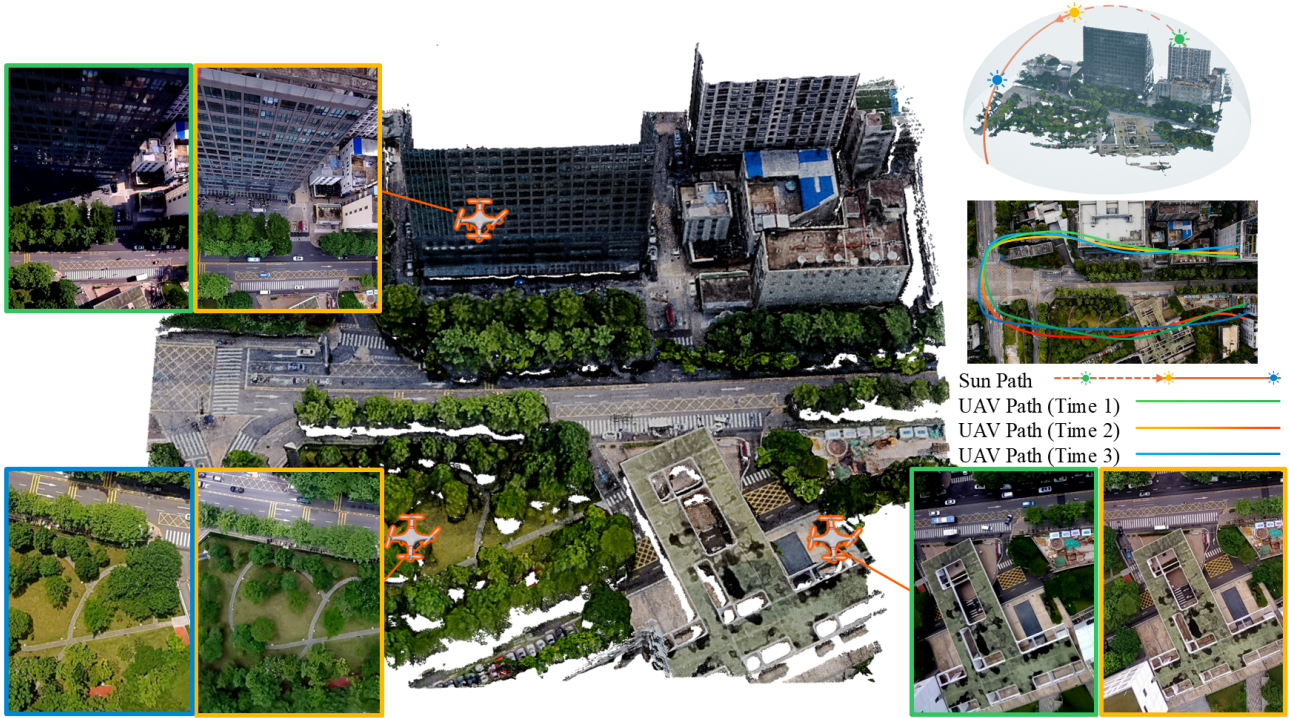[4]Meituan Academy of Robotics Shenzhen

Figure 1. Overview of the UAVLight benchmark. Each scene is captured by low-altitude UAV flights along fixed waypointed trajectories at multiple times of day. Our benchmark records natural illumination changes along consistent geometry and viewpoints, enabling quantitative evaluation of illumination-robust reconstruction and relighting.

Abstract

Illumination inconsistency is a fundamental challenge in multi-view 3D reconstruction. Variations in sunlight direction, cloud cover, and shadows break the constant-lighting assumption underlying both classical multi-view stereo (MVS) and structure from motion (SfM) pipelines and recent neural rendering methods, leading to geometry drift, color inconsistency, and shadow imprinting. This issue is especially critical in UAV-based reconstruction, where long flight durations and outdoor environments make lighting changes unavoidable. However, existing datasets either restrict capture to short time windows, thus lacking meaningful illumination diversity, or span months and seasons,

---

[*]Corresponding author.

1

where geometric and semantic changes confound the isolated study of lighting robustness. We introduce UAVLight, a controlled-yet-real benchmark for illumination-robust 3D reconstruction. Each scene is captured along repeatable, geo-referenced flight paths at multiple fixed times of day, producing natural lighting variation under consistent geometry, calibration, and viewpoints. With standardized evaluation protocols across lighting conditions, UAVLight provides a reliable foundation for developing and benchmarking reconstruction methods that are consistent, faithful, and relightable in real outdoor environments.

1. Introduction

Recent neural 3D reconstruction methods have advanced from classical SfM [28] and MVS [18, 36] to neural fields [21, 22] and Gaussian Splatting [12, 25], achieving photorealistic rendering and accurate geometry from casual multi-view imagery. However, most widely used benchmarks [1, 14, 36] implicitly assume stationary illumination: scenes are captured within minutes under nearly fixed lighting. In contrast, 3D reconstruction with UAV often lasts for hours or is conducted at various times of a day, during which the solar position, intensity, and atmospheric conditions vary significantly. Such non-stationary outdoor illumination deviates from the constant-lighting assumption, leading to geometry drift, view-dependent color shifts, shadow imprinting in reflectance, and unstable relighting.

Existing approaches can be broadly grouped into the following two categories. (1) *Implicit appearance modeling* augments neural fields with per-view/per-ray latents to absorb exposure, white balance, shadows, and weather-induced variations [15, 19, 37, 38]. While this improves robustness "in the wild" but offers limited physical interpretability and unreliable relighting. (2) *Explicit lighting estimation* factorizes appearance into reflectance and illumination via inverse rendering, enabling physically grounded relighting and shadow reasoning, but it requires strong priors (e.g., sun–sky models [5]), accurate calibration, and is brittle under auto-exposure [11, 16, 27].

Recent studies have integrated 3D reconstruction into UAV scenarios [8, 30, 31]. However, there remains no dataset that systematically elicits, isolates, and evaluates performance under time-varying sunlight while keeping geometry and viewpoints consistent. A few recent datasets capture multiple lighting conditions, but are either object-centric with limited geometric complexity [33] or span long temporal windows [27], during which geometry, vegetation, and transient objects evolve alongside illumination. These uncontrolled variations confound illumination effects, hindering isolation, quantification, and fair comparison of illumination robustness across methods. Consequently, research progress on *illumination-robust reconstruction* re-

mains difficult to measure, and evaluations between implicit and explicit methods are often inconclusive.

To isolate illumination effects while preserving real-world realism, we adopt three principles: (i) focus on outdoor UAV ground scenes primarily lit by sunlight, avoiding indoor or multi-source lighting confounders; (ii) capture at consistent time slots over short periods (e.g., consecutive days) to reduce non-illumination changes such as layout, vegetation, and human activity; (iii) repeat consistent, way-pointed flight trajectories to obtain comparable viewpoints and scene coverage across captures. Furthermore, nadir-oriented flight plans greatly limit sky pixels, reducing HDR sky ambiguity and improving cross-method comparability.

Guided by these principles, we introduce *UAVLight*, a benchmark and dataset that supports 3D reconstruction under realistic, time-varying natural lighting while controlling geometry and viewpoint comparability. For reliable quantitative evaluation, we provide high-quality, geo-referenced point clouds as a geometric reference. Beyond raw data, UAVLight standardizes splits, tasks, and metrics to jointly assess geometry, cross-time photometric consistency, and relighting stability. UAVLight advances illumination-robust 3D reconstruction by providing:

- **A Controlled-Yet-Real Benchmark:** multi-time-of-day UAV captures (∼5 per scene) along repeated, GPS-waypointed trajectories with consistent intrinsics and comparable viewpoints, isolating time-varying sunlight under real-world conditions;
- **Reliable Geometric Reference:** high-quality and geo-referenced point clouds enabling absolute, scene-scale accuracy assessment;
- **Novel Standardized Evaluations:** unified splits, tasks, and metrics that jointly measure reconstruction fidelity, cross-time photometric consistency with representative baselines from both implicit appearance modeling and explicit inverse-rendering approaches.

2. Existing Benchmarks

As summarized in Table 1, existing illumination-aware 3D reconstruction datasets can be organized along six key axes capturing realism, controllability, and diversity: (1) content (indoor, object-centric, or outdoor), (2) target task (single- or multi-view reconstruction), (3) lighting consistency within a sequence, (4) illumination source (synthetic, natural, or controlled), (5) number of lighting conditions per scene, and (6) number of included scenes. These dimensions together form a concise taxonomy as benchmarks.

Synthetic and object-centric datasets mainly emphasize controlled appearance analysis. NeRF Synthetic [21] and TensoIR [9] offer clean geometry and perfectly specified lighting, useful for isolating modeling errors but lacking real-world variability. Object-centric multi-view datasets such as OWL [33] and OpenIllumination [17] enable ma-

Table 1. A taxonomy of existing datasets.

Dataset	Content	Purpose	Same-light (per seq.)	Light source	# Illum.	# Scenes
NeRF Synthetic[21]	Objects	Multi-view	-	Synthetic	-	8
TensoIR[9]	Objects	Multi-view	-	Synthetic	-	4
Objects with Lights[33]	Objects	Multi-view	Yes	Natural	3	8
OpenIllumination[17]	Objects	Multi-view	-	Light stage	13 pattern+142OLAT	64
LSMI[13]	Indoor	Single-view	-	Spotlight	1-3	2700
Multi-illumination in the Wild[23]	Indoor	Single-view	-	Spotlight	25	1000
Phototourism[32]	Outdoor	Multi-view	No	Natural	-	13
NeRF-OSR[27]	Outdoor	Multi-view	Yes	Natural	5+	9
Ours	**UAV**	**Multi-view**	**Yes**	**Natural**	**3-11**	**18**

Table 2. Data acquisition and reconstruction configuration.

Component	Specification
UAV platform	DJI flight system with RTK positioning
Camera type	Third-party global-shutter RGB camera
Resolution	1280×960 pixels
Frame rate	30 fps
Exposure	Automatic

terial and relighting studies; the former captures under natural light with limited conditions, while the latter employs dense light-stage setups with high photometric control but small geometric scope.

Indoor single-view datasets, including LSMI [13] and Multi-Illumination Images in the Wild [23], focus on per-image illumination estimation under diverse artificial sources. However, they lack multi-view consistency and stable geometry, making them unsuitable for evaluating cross-view reconstruction or lighting disentanglement.

Outdoor reconstruction datasets emphasize geometry but assume fixed illumination. MipNeRF-360 [1] and Tanks&Temples [14] are captured within short time windows, limiting illumination diversity. Phototourism [32] aggregates Internet photos with uncontrolled exposures and timestamps, providing variety in viewpoint but not in lighting conditions. NeRF-OSR [27] introduces multiple sunlight settings per scene but collects data over months or years, during which geometry and semantics drift, complicating fair illumination evaluation.

Our Position. We design an outdoor, scene-level, multi-view UAV dataset captured under natural sunlight, where frames within each sequence share consistent illumination. Each scene includes 3–11 time slots along fixed waypointed trajectories across 18 diverse scenes. This configuration maintains real-world realism while controlling confounding factors, enabling systematic evaluation of illumination robustness and relighting stability.

3. Dataset Design Principles

UAVLight is designed to isolate light as the primary varying factor while maintaining consistent geometry and views. This is achieved through three key principles, enabling fair benchmarking of reconstruction and relighting methods.

Low-altitude Imaging. Flights are conducted at low altitudes with nadir or oblique views, where direct sunlight dominates and diffuse components are negligible. This yields physically interpretable lighting changes governed by the solar position.

Repeated Trajectories. Each scene is captured along identical waypointed paths at several fixed times of day, ensuring comparable viewpoint coverage and parallax across flights. Crucially, in large-scale outdoor scenes, illumination within a single time slot can be treated as uniform—sun position, cast-shadow directions, and ambient contributions remain stable over the short flight interval.

Real-Time Kinematic (RTK)-Based Registration. All cameras use RTK positioning to provide metric-scale priors for SfM and MVS, reducing drift and aligning reconstructions across time in a shared world frame.

4. Data Collection

UAVLight is captured through a standardized four-stage process, including data acquisition, frame sampling and reconstruction, post-processing, and sunlight calculation.

Data Acquisition. As shown in Table 2, we use a DJI flight platform with RTK positioning and a global-shutter RGB camera. Each scene is captured by repeating the same waypointed trajectory at multiple time slots, ensuring matched viewpoints while allowing natural changes in sunlight direction and intensity. RTK logs provide timestamp, latitude, longitude, and altitude for every frame, yielding centimeter-level pose accuracy. The onboard camera records 1280×960 images at 30 fps with automatic exposure and a global shutter, avoiding rolling-shutter artifacts.
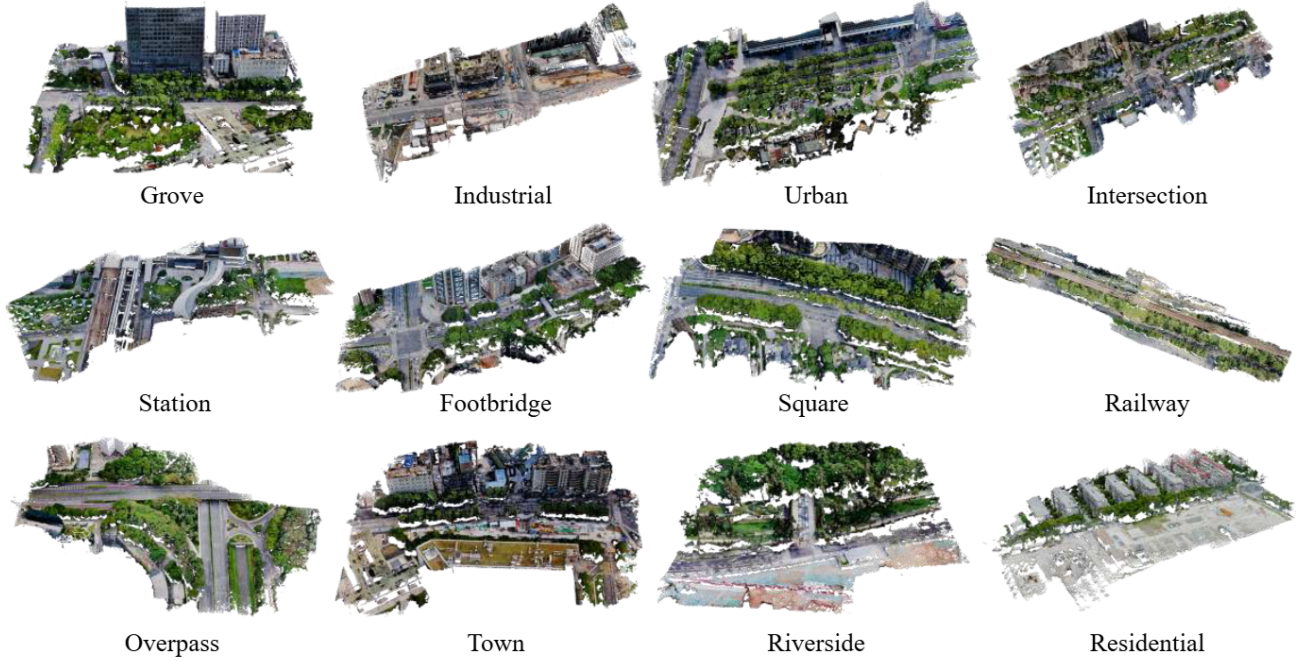
Figure 2. Visualization of representative dense point clouds from 12 selected scenes in our benchmark.

Table 3. **UAV-Light scene statistics.** Each scene is captured under multiple natural illumination conditions along repeated flight trajectories.

Scene	Area (m^2)	Traj. (m)	#Images	#Illum.
Residential	37044	300	267	3
Town	21624	200	194	8
Grove	20900	190	253	11
Railway	27280	440	222	5
Riverside	22733	180	224	7
Square	26985	260	233	6
Footbridge	39776	350	326	6
Industrial	42130	380	234	3
Intersection	31110	300	278	5
Urban	32239	310	239	5
Station	37600	380	264	6
Overpass	39308	310	290	5
Road	32120	290	126	3
Park	49920	520	336	6
SportsField	69204	470	286	3
Industrial2	18542	260	166	6
Grove2	32120	290	208	10
Road2	26790	290	239	5

Frame Sampling and Reconstruction. To balance spatial coverage and computational efficiency, we uniformly sample video frames at 1 fps. Each sampled image is tagged with its precise RTK-GNSS position. Building upon the Structure-from-Motion framework [28], we integrate these geospatial priors into the reconstruction pipeline to enhance geo-registration. Our approach extends the grouped bundle adjustment concept by incorporating a robust RTK position constraint, a strategy motivated by using GNSS data for improving accuracy in UAV photogrammetry [24]. The total energy function we minimize is:

$$E_{\text{total}} = E_{\text{group}} + \sum_i \kappa_i \left\| \mathbf{c}_i - \mathbf{t}_{\text{RTK}_i} \right\|_2^2, \qquad (1)$$

where the grouped bundle adjustment (BA) cost E_{group} is defined as:

$$E_{\text{group}} = \sum_j \rho_j \left(\left\| \pi_g(\mathbf{G}_r, \mathbf{P}_c, \mathbf{X}_k) - \mathbf{x}_{jk} \right\|_2^2 \right). \qquad (2)$$

E_{group} represents the visual reprojection error within camera groups, reducing the number of free parameters. The second term enforces a soft constraint that penalizes deviations between the optimized camera center $\mathbf{c}_i$ and its corresponding RTK measurement $\mathbf{t}_{\text{RTK}_i}$, with κ_i controlling the constraint strength. This combination significantly improves pose estimation accuracy and scale consistency, leading to more robust MVS reconstruction and geometrically consistent models across different flight passes. We also output the dense point clouds, as shown in Figure 2.

Post Processing. Following automatic data parsing, we conduct a manual quality assessment to filter out frames that are suboptimal for 3D reconstruction. This includes removing images affected by motion blur [10], significant over-exposure or extreme shadows that compromise feature matching [20], and those dominated by non-Lambertian or poorly-textured surfaces like large water bodies [29]. The
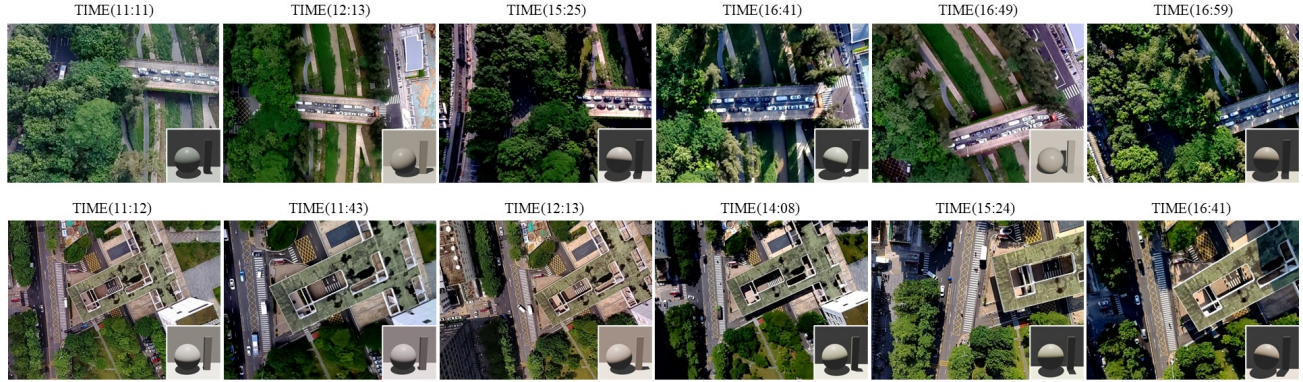
4

Figure 3. Illustration of illumination variations across similar viewpoints at different times of day. The bottom-right panel shows the corresponding ground-truth sunlight directions computed from GPS and timestamps.
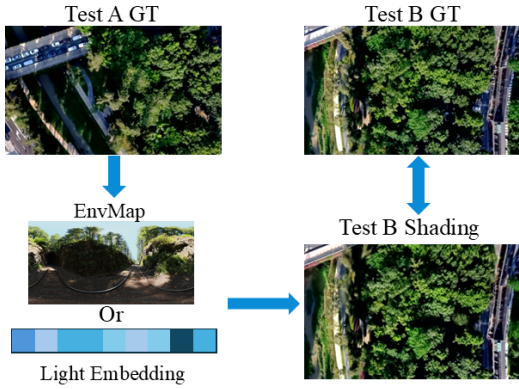

Figure 4. Paired cross-light protocol used for evaluating methods. For each time slot, lighting is estimated from one subset of views and applied to another subset captured under the same time slot.

curated set of high-quality frames is then processed using a standard SfM-based undistortion pipeline [28] to correct for lens distortions and ensure precise spatial consistency. This hybrid manual-automatic cleaning procedure guarantees that the final image collection is both geometrically reliable and photometrically suitable for the subsequent relighting and reconstruction evaluations.

Sunlight Ground Truth. In addition to dense pointclouds and appearance annotations, UAVLight provides the GT direction of sunlight for each time slot, as shown in Figure 3. Assuming sunlight as a global directional source [6], the direction is computed from the timestamp and geographic coordinates recorded during UAV acquisition, following the standard solar position algorithm [26].

Given a timestamp t (in Universal Time Coordinated, UTC) and the camera's geographic coordinates—longitude λ (in degrees, positive east) and latitude ϕ (in degrees, positive north)—we first compute the solar altitude angle α_{sun} (elevation above the horizon) and the solar azimuth angle γ_{sun} (clockwise from true North) using the algorithm in [26]. The solar zenith angle θ_{sun}, complementary to the altitude angle, is given by: $\theta_{\text{sun}} = 90° - \alpha_{\text{sun}}$.

The unit direction vector $\mathbf{s}_{\text{ENU}}$ pointing towards the sun in the local East–North–Up (ENU) coordinate system at the camera location is then defined as:

$$\begin{aligned} s_{\text{E}} &= \sin(\gamma_{\text{sun}}), \\ s_{\text{N}} &= \cos(\gamma_{\text{sun}}), \\ s_{\text{U}} &= \sin(\alpha_{\text{sun}}) = \cos(\theta_{\text{sun}}). \end{aligned} \quad (3)$$

These components represent the direction's projection onto the East, North, and Up axes, respectively. We assume the azimuth γ_{sun} is measured clockwise from North.

Finally, this sun direction vector $\mathbf{s}_{\text{ENU}}$ is transformed into the global coordinate system of the COLMAP model, $\mathbf{s}_{\text{Colmap}}$, using the rotation matrix $\mathbf{R}$ that aligns the local ENU frame with the COLMAP [28] coordinate frame:

$$\mathbf{s}_{\text{Colmap}} = \mathbf{R}\,\mathbf{s}_{\text{ENU}}. \quad (4)$$

The rotation matrix $\mathbf{R}$ is derived from the camera's orientation and position within the COLMAP reconstruction. Such physically grounded sunlight annotation provides a reliable supervision signal for downstream tasks, including outdoor lighting estimation [2, 6, 35], inverse rendering [3, 4], and relightable neural reconstruction [11].

5. Scenes

UAVLight comprises a total of 18 real-world outdoor scenes, each covering a large spatial area and exhibiting diverse geometric layouts, materials, and environmental contexts. This diversity ensures that illumination effects manifest richly through cast shadows, specular highlights, diffuse shading gradients, and global illumination interactions. The outdoor environments in UAVLight (Table 3) include:

- **Natural Vegetation Scenes**: (*Park*, *Grove*, and *Grove2*) Capture and feature high-density natural vegetation foliage. These elements create dense occlusion, dappled light, complex soft-shadow behavior, and spatially varying leaf reflectance.

Table 4. Quantitative results on Scenes 1–6. Evaluated using PSNR ↑, SSIM ↑, and LPIPS ↓.

Time	Method	Town			Residential			Riverside			Grove			Railway			Square		
		PSNR	SSIM	LPIPS	PSNR	SSIM	LPIPS	PSNR	SSIM	LPIPS	PSNR	SSIM	LPIPS	PSNR	SSIM	LPIPS	PSNR	SSIM	LPIPS
353 hr	NeRF-W	19.63	0.653	0.410	20.74	0.733	0.414	17.34	0.612	0.448	17.83	0.595	0.430	16.37	0.480	0.551	19.02	0.546	0.443
179 hr	NeRF-OSR	18.95	0.506	0.489	20.77	0.663	0.505	18.73	0.536	0.525	17.86	0.518	0.478	15.73	0.391	0.753	18.18	0.453	0.573
42 hr	GS-W	22.27	0.787	0.161	25.66	0.851	0.144	22.08	0.775	0.182	21.81	0.779	0.144	16.35	0.570	0.361	23.16	0.770	0.124
46 hr	W-GS	23.95	0.792	0.175	23.62	0.816	0.234	21.90	0.747	0.226	22.49	0.778	0.164	18.34	0.606	0.382	23.62	0.746	0.168
36 hr	LumiGS	23.59	0.841	0.128	25.14	0.851	0.161	23.02	0.809	0.156	21.27	0.765	0.164	17.97	0.624	0.299	24.31	0.791	0.123

Table 5. Quantitative results on Scenes 7–12. Evaluated using PSNR ↑, SSIM ↑, and LPIPS ↓.

Time	Method	Footbridge			Industrial			Intersection			Urban			Station			Overpass		
		PSNR	SSIM	LPIPS	PSNR	SSIM	LPIPS	PSNR	SSIM	LPIPS	PSNR	SSIM	LPIPS	PSNR	SSIM	LPIPS	PSNR	SSIM	LPIPS
356 hr	NeRF-W	17.25	0.515	0.487	17.78	0.612	0.461	16.39	0.484	0.497	17.57	0.502	0.469	18.52	0.565	0.474	18.52	0.634	0.409
181hr	NeRF-OSR	17.13	0.428	0.591	17.50	0.518	0.544	16.81	0.390	0.583	17.03	0.392	0.602	18.46	0.495	0.586	20.45	0.590	0.430
43hr	GS-W	17.85	0.608	0.294	19.33	0.762	0.183	19.98	0.724	0.175	19.49	0.688	0.205	22.83	0.785	0.131	22.40	0.787	0.127
47hr	W-GS	17.45	0.562	0.458	16.63	0.676	0.337	21.38	0.708	0.226	21.50	0.705	0.218	22.23	0.756	0.177	23.08	0.803	0.143
35hr	LumiGS	20.89	0.742	0.17	20.34	0.791	0.158	23.04	0.805	0.127	21.26	0.743	0.164	23.11	0.805	0.123	22.33	0.813	0.127

- **Urban and Residential Areas**: (*Residential*, *Urban*, and *Town*) Combine rich and varied geometry (e.g., multi-level facades, varied rooftops, and narrow streets) and heterogeneous material reflectance (i.e., metallic surfaces, windows, and pavements). These elements combine to create deep cast-shadow occlusions and articulated shadow boundaries.
- **Open Public Spaces**: (*Square* and *SportsField*) Feature large-scale, geometrically simple open areas with minimal occlusion and uniform surface reflectance. These elements provide clear shadow boundaries and a uniform light response.
- **Industrial Sites**: (*Industrial* and *Industrial2*) Capture and feature large open areas mixed with dense, repetitive structures such as scaffolding and piping. Metallic surfaces produce anisotropic highlights and strong directional shading, posing difficulties for both material decomposition and geometric recovery.
- **Transportation Infrastructure**: (*Road1*, *Road2*, *Intersection*, *Footbridge*, *Station*, *Overpass*, and *Railway*) Combine wide ground regions with multi-level structures. These scenes exhibit long-range shadows and sharp light transitions that violate the constant-lighting assumption.
- **Riverside Regions**: (*Riverside*) Contain strong water-surface specularities, vegetation-induced subsurface scattering, and long cast shadows from bridges, establishing a challenging testbed for non-Lambertian reflectance.

6. Experiments

We present a benchmark for inverse rendering that enables fair evaluation of 3D reconstruction under various lighting conditions without requiring external environment maps.

6.1. Experiment Design

Existing evaluation protocols generally fall into two categories. (1) [19], and its followers adopt a half-split protocal: estimate lighting from one half of the views and evaluate on the other half. However, using only half of the views may provide incomplete lighting cues, causing the learned embedding to overfit view-specific appearance. (2) Methods such as [27] evaluated with calibrated environment maps, which are physically grounded but are expensive to capture for all time slots and difficult to apply to large outdoor areas. As shown in Figure 4, to support both implicit and explicit-illumination approaches, we adopt a paired cross-illumination setup in which lighting is estimated from one subset of views and evaluated on another within the same time slot. This ensures consistent geometry while isolating illumination as the only varying factor without GT envmap.

6.2. Data Splits and Reproducibility

To ensure fair comparison and reproducibility, UAVLight follows a standardized train/val/test split across different time slots, avoiding temporal leakage. For each test slot, camera views are further divided into two subsets, A_t and B_t, matched by altitude and view angle to enable unbiased cross-illumination evaluation. We release all configuration details—fixed random seeds, A/B view indices, exposure normalization parameters, and an official evaluation script—to guarantee consistent and repeatable results.

6.3. Baselines

We evaluate five representative baselines, which fall into two broad categories: **Implicit illumination modeling.** These approaches encode lighting variations implicitly through learned latent features, without explicitly recovering scene illumination. This category includes GS-W [38], WildGaussians [15], and NeRF-W [19]. **Explicit illumination modeling.** These inverse-rendering-based methods recover shared geometry and materials across time, while estimating per-capture lighting for relighting. This category includes LumiGauss [11] and NeRF-OSR [27].
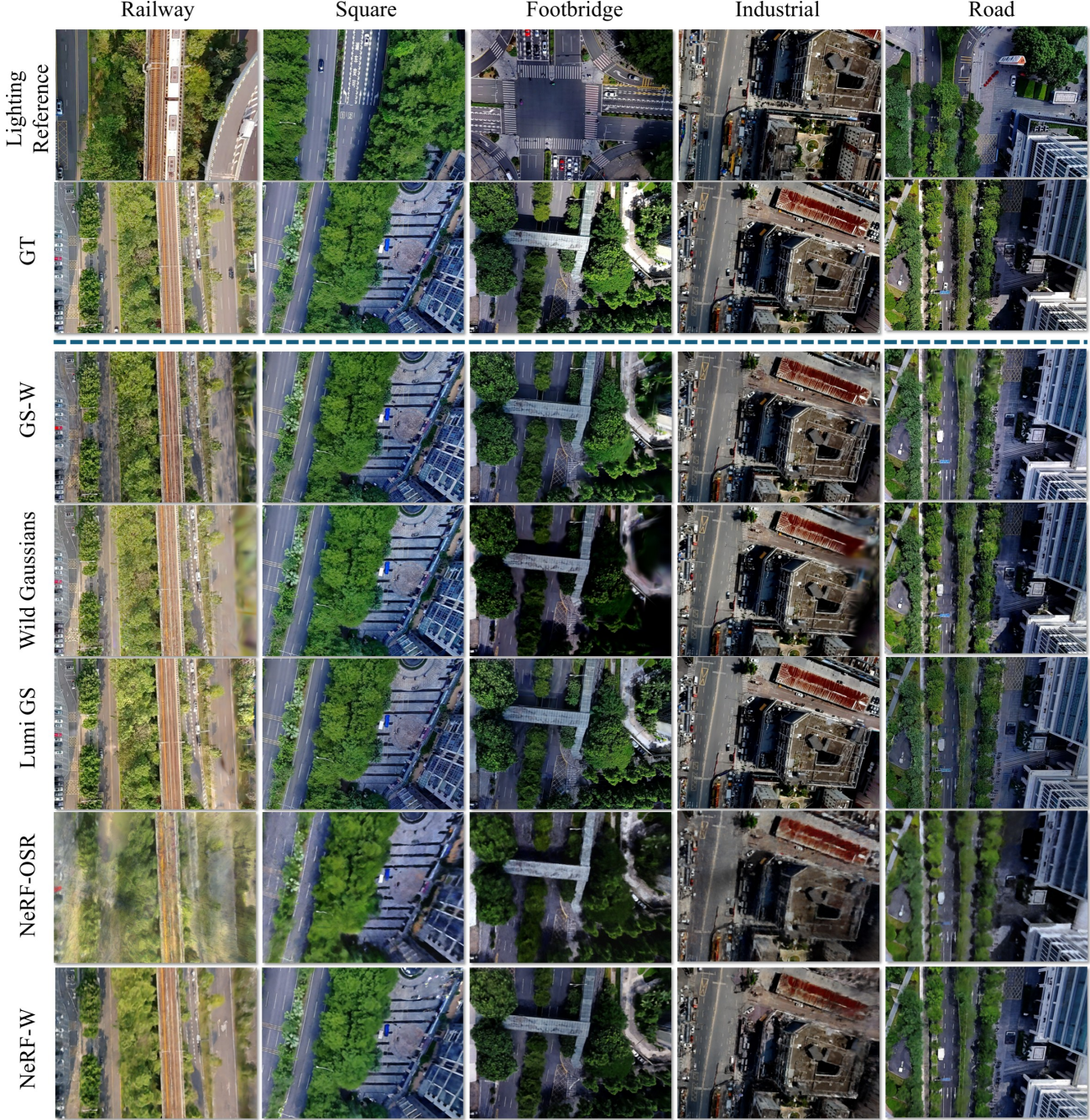
Figure 5. Visualization of the reconstruction results from different baselines on five UAVLight scenes.

7. Results

We evaluate all baselines across 12 representative scenes in UAVLight. Our goal is to examine how existing 3D reconstruction and inverse rendering approaches behave under real-world illumination variations, which previous benchmarks have struggled with. Quantitative results are summarized in Tables 4 and 5, and visual comparisons are presented in Figures 5 and 6. The remaining 6 scenes and additional experimental analysis are detailed in the supplement.

7.1. Quantitative Analysis

Across all scenes, clear and interpretable trends emerge. Gaussian-based methods achieve the strongest performance in standard metrics (PSNR [7], SSIM [34], LPIPS [39]), confirming their stability under multi-view reconstruction. More importantly, explicit illumination models (LumiGauss
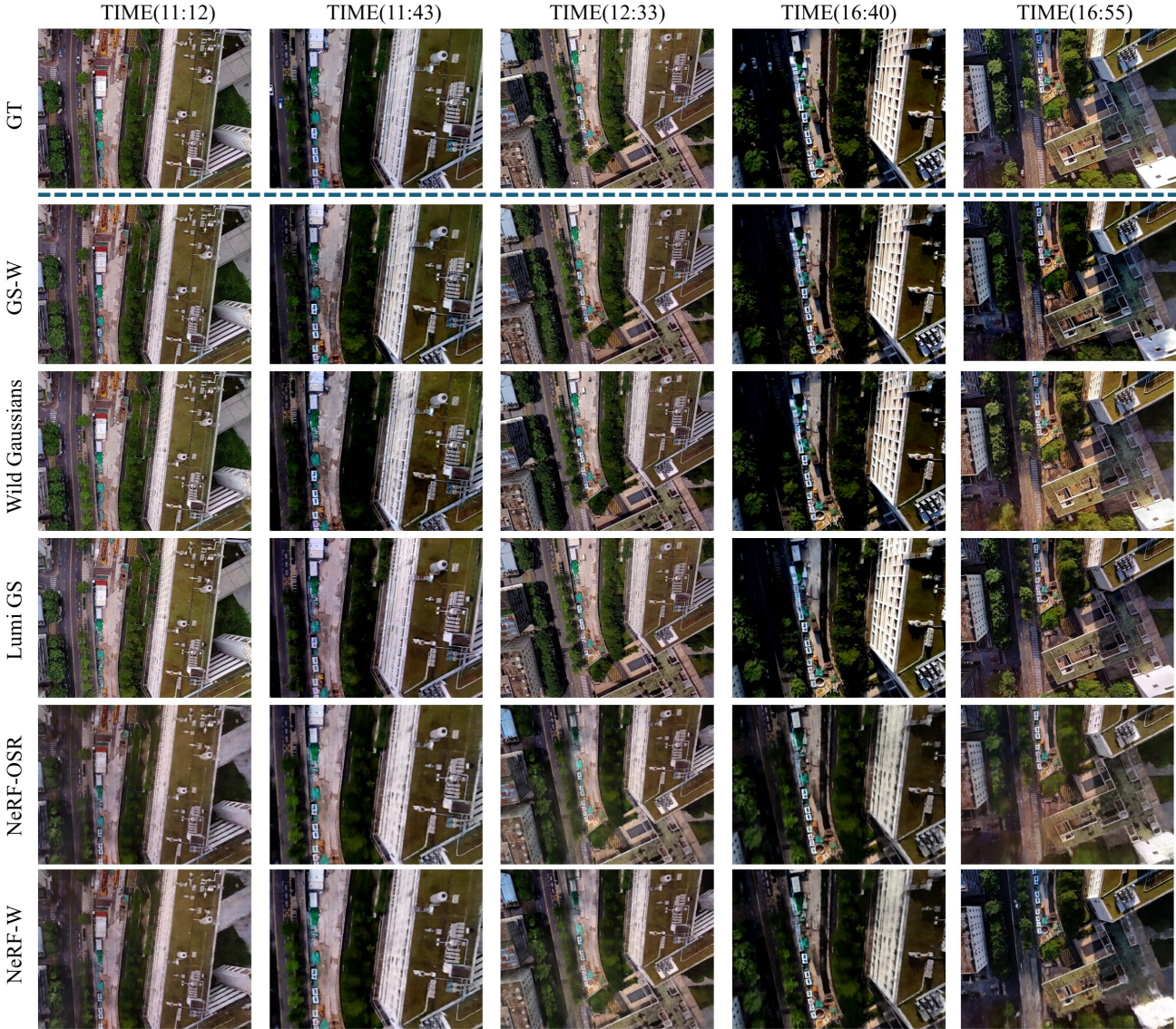
7

Figure 6. Visualization of the reconstruction results from different baselines on Town with five different time slots.

[11]) consistently outperform implicit ones (Gaussian Wild [38], WildGaussians [15], NeRF-W [19]) when evaluated across different illumination slots. This gap highlights a key difficulty revealed by UAVLight: methods that entangle lighting with color struggle to maintain geometry-material consistency under illumination changes, whereas explicit decompositions provide more reliable supervision.

7.2. Qualitative Analysis

The qualitative results further illustrate the role of UAVLight in exposing illumination-dependent failure modes. *Footbridge* in Figure 5 shows that implicit methods, though sometimes sharper around high-frequency areas, such as shadow boundaries, often imprint shadows into

albedo or distort geometry when light changes across time of day. In contrast, explicit illumination methods produce more coherent soft shadows. Figure 6 shows that these trends persist across diverse lighting conditions. In particular, at TIME (16:55), GS-W produces sharper shadows, whereas LumiGauss yields shading closer to ground truth.

7.3. Overall Observation

The results show that UAVLight not only distinguishes the strengths of Gaussian-based reconstruction, but also reveals the fundamental trade-offs between implicit and explicit illumination modeling. Explicit approaches exhibit stronger disentanglement and more stable multi-light reconstruction, while implicit ones capture certain high-frequency effects

but are more prone to entanglement-induced artifacts. More results are provided in the supplemental materials.

8. Conclusion

In summary, UAVLight establishes the first benchmark for multi-lighting reconstruction in real-world UAV scenes. Through capturing consistent frames across natural lighting variations, it enables a fair comparison of implicit and explicit lighting models. Future extensions of UAVLight include expanding illumination diversity (clouds, seasons, atmospheric variation), and developing real-to-sim paired versions for outdoor simulation and embodied-AI research.

References

[1] Jonathan T Barron, Ben Mildenhall, Dor Verbin, Pratul P Srinivasan, and Peter Hedman. MIP-NeRF 360: Unbounded Anti-Aliased Neural Radiance Fields. In *Proceedings of the IEEE/CVF Conference on Computer Vision and Pattern Recognition*, pages 5470–5479, 2022. 2, 3

[2] Christophe Bolduc, Yannick Hold-Geoffroy, and Jean-François Lalonde. GaSLight: Gaussian Splats for Spatially-Varying Lighting in HDR. In *Proceedings of the IEEE/CVF International Conference on Computer Vision (ICCV)*, pages 29120–29130, 2025. 5

[3] HONGZE CHEN, Zehong Lin, and Jun Zhang. GI-GS: Global Illumination Decomposition on Gaussian Splatting for Inverse Rendering. In *The Thirteenth International Conference on Learning Representations*. 5

[4] Kang Du, Zhihao Liang, Yulin Shen, and Zeyu Wang. GS-ID: Illumination Decomposition on Gaussian Splatting via Adaptive Light Aggregation and Diffusion-Guided Material Priors. In *Proceedings of the IEEE/CVF International Conference on Computer Vision*, pages 26220–26229, 2025. 5

[5] James AD Gardner, Evgenii Kashin, Bernhard Egger, and William AP Smith. The Sky's the Limit: Relightable Outdoor Scenes via a Sky-Pixel Constrained Illumination Prior and Outside-In Visibility. In *European Conference on Computer Vision*, pages 126–143. Springer, 2024. 2

[6] Yannick Hold-Geoffroy, Kalyan Sunkavalli, Sunil Hadap, Emiliano Gambaretto, and Jean-François Lalonde. Deep Outdoor Illumination Estimation. In *Proceedings of the IEEE Conference on Computer Vision and Pattern Recognition*, pages 7312–7321, 2017. 5

[7] Alain Hore and Djemel Ziou. Image Quality Metrics: PSNR vs. SSIM. In *2010 20th International Conference on Pattern Recognition*, pages 2366–2369. IEEE, 2010. 7

[8] Léonard Jaillet, Juan Cortés, and Thierry Siméon. Sampling-Based Path Planning on Configuration-Space Costmaps. *IEEE Transactions on Robotics*, 26(4):635–646, 2010. 2

[9] Haian Jin, Isabella Liu, Peijia Xu, Xiaoshuai Zhang, Song-fang Han, Sai Bi, Xiaowei Zhou, Zexiang Xu, and Hao Su. Tensoir: Tensorial Inverse Rendering. In *Proceedings of the IEEE/CVF Conference on Computer Vision and Pattern Recognition*, pages 165–174, 2023. 2, 3

[10] Neel Joshi, C Lawrence Zitnick, Richard Szeliski, and David J Kriegman. Image Deblurring and Denoising Using Color Priors. In *2009 IEEE Conference on Computer Vision and Pattern Recognition*, pages 1550–1557. IEEE, 2009. 4

[11] Joanna Kaleta, Kacper Kania, Tomasz Trzciński, and Marek Kowalski. LumiGauss: Relightable Gaussian Splatting in the Wild. In *2025 IEEE/CVF Winter Conference on Applications of Computer Vision (WACV)*, pages 1–10. IEEE, 2025. 2, 5, 6, 8

[12] Bernhard Kerbl, Georgios Kopanas, Thomas Leimkühler, and George Drettakis. 3D Gaussian Splatting for Real-Time Radiance Field Rendering. *ACM Trans. Graph.*, 42(4):139–1, 2023. 2

[13] Dongyoung Kim, Jinwoo Kim, Seonghyeon Nam, Dongwoo Lee, Yeonkyung Lee, Nahyup Kang, Hyong-Euk Lee, Byung-gIn Yoo, Jae-Joon Han, and Seon Joo Kim. Large Scale Multi-Illuminant (LSMI) Dataset for Developing White Balance Algorithm under Mixed Illumination. In *Proceedings of the IEEE/CVF International Conference on Computer Vision*, pages 2410–2419, 2021. 3

[14] Arno Knapitsch, Jaesik Park, Qian-Yi Zhou, and Vladlen Koltun. Tanks and Temples: Benchmarking Large-Scale Scene Reconstruction. *ACM Transactions on Graphics (ToG)*, 36(4):1–13, 2017. 2, 3

[15] Jonas Kulhanek, Songyou Peng, Zuzana Kukelova, Marc Pollefeys, and Torsten Sattler. WildGaussians: 3D gaussian splatting in the wild. In *Proceedings of the 38th International Conference on Neural Information Processing Systems*, 2024. 2, 6, 8

[16] Jingzhi Li, Zongwei Wu, Eduard Zamfir, and Radu Timofte. Recap: Better Gaussian Relighting with Cross-Environment Captures. In *Proceedings of the Computer Vision and Pattern Recognition Conference*, pages 21307–21316, 2025. 2

[17] Isabella Liu, Linghao Chen, Ziyang Fu, Liwen Wu, Haian Jin, Zhong Li, Chin Ming Ryan Wong, Yi Xu, Ravi Ramamoorthi, Zexiang Xu, et al. OpenIllumination: A Multi-Illumination Dataset for Inverse Rendering Evaluation on Real Objects. *Advances in Neural Information Processing Systems*, 36:36951–36962, 2023. 2, 3

[18] Mehdi Maboudi, MohammadReza Homaei, Soohwan Song, Shirin Malihi, Mohammad Saadatseresht, and Markus Gerke. A Review on Viewpoints and Path Planning for UAV-Based 3-D Reconstruction. *IEEE Journal of Selected Topics in Applied Earth Observations and Remote Sensing*, 16: 5026–5048, 2023. 2

[19] Ricardo Martin-Brualla, Noha Radwan, Mehdi SM Sajjadi, Jonathan T Barron, Alexey Dosovitskiy, and Daniel Duck-worth. NeRF in the Wild: Neural Radiance Fields for Unconstrained Photo Collections. In *Proceedings of the IEEE/CVF Conference on Computer Vision and Pattern Recognition*, pages 7210–7219, 2021. 2, 6, 8

[20] Yasuyuki Matsushita and Stephen Lin. Radiometric Calibration from Noise Distributions. In *2007 IEEE Conference on Computer Vision and Pattern Recognition*, pages 1–8. Ieee, 2007. 4

[21] Ben Mildenhall, Pratul P Srinivasan, Matthew Tancik, Jonathan T Barron, Ravi Ramamoorthi, and Ren Ng. NeRF:

Representing Scenes as Neural Radiance Fields for View Synthesis. *Communications of the ACM*, 65(1):99–106, 2021. 2, 3

[22] Yuhang Ming, Xingrui Yang, Weihan Wang, Zheng Chen, Jinglun Feng, Yifan Xing, and Guofeng Zhang. Benchmarking Neural Radiance Fields for Autonomous Robots: An Overview. *Engineering Applications of Artificial Intelligence*, 140:109685, 2025. 2

[23] Lukas Murmann, Michael Gharbi, Miika Aittala, and Fredo Durand. A Dataset of Multi-Illumination Images in the Wild. In *Proceedings of the IEEE/CVF International Conference on Computer Vision*, pages 4080–4089, 2019. 3

[24] Eise Wiebe Nota, W Nijland, and Tjalling de Haas. Improving UAV-SfM Time-Series Accuracy by Co-Alignment and Contributions of Ground Control or RTK Positioning. *International Journal of Applied Earth Observation and Geoinformation*, 109:102772, 2022. 4

[25] Kai Qin, Jing Li, Sisi Zlatanova, Haitao Wu, Yin Gao, Yuchen Li, Sizhe Shen, Xiangjun Qu, Zhiyuan Yang, Zhenxin Zhang, Banghui Yang, and Shaoyi Wang. Novel UAV-based 3D Reconstruction Using Dense LiDAR Point Cloud and Imagery: A Geometry-Aware 3D Gaussian Splatting Approach. *International Journal of Applied Earth Observation and Geoinformation*, 140:104590, 2025. 2

[26] Ibrahim Reda and Afshin Andreas. Solar Position Algorithm for Solar Radiation Applications. Technical Report NREL/TP-560-34302, National Renewable Energy Laboratory (NREL), 2008. 5

[27] Viktor Rudnev, Mohamed Elgharib, William Smith, Lingjie Liu, Vladislav Golyanik, and Christian Theobalt. NeRF for Outdoor Scene Relighting. In *European Conference on Computer Vision*, pages 615–631. Springer, 2022. 2, 3, 6

[28] Johannes L Schonberger and Jan-Michael Frahm. Structure-From-Motion Revisited. In *Proceedings of the IEEE Conference on Computer Vision and Pattern Recognition*, pages 4104–4113, 2016. 2, 4, 5

[29] Steven M Seitz, Brian Curless, James Diebel, Daniel Scharstein, and Richard Szeliski. A Comparison and Evaluation of Multi-View Stereo Reconstruction Algorithms. In *2006 IEEE Computer Society Conference on Computer Vision and Pattern Recognition (CVPR'06)*, pages 519–528. IEEE, 2006. 4

[30] Zhexiong Shang and Zhigang Shen. Topology-Based UAV Path Planning for Multi-View Stereo 3D Reconstruction of Complex Structures. *Complex & Intelligent Systems*, 9(1): 909–926, 2023. 2

[31] Neil Smith, Nils Moehrle, Michael Goesele, and Wolfgang Heidrich. Aerial Path Planning for Urban Scene Reconstruction: A Continuous Optimization Method and Benchmark. 2018. 2

[32] Noah Snavely, Steven M Seitz, and Richard Szeliski. Photo Tourism: Exploring Photo Collections in 3D. In *ACM siggraph 2006 papers*, pages 835–846. 2006. 3

[33] Benjamin Ummenhofer, Sanskar Agrawal, Rene Sepulveda, Yixing Lao, Kai Zhang, Tianhang Cheng, Stephan Richter, Shenlong Wang, and German Ros. Objects with Lighting: A Real-World Dataset for Evaluating Reconstruction and Rendering for Object Relighting. In *2024 International Conference on 3D Vision (3DV)*, pages 137–147. IEEE, 2024. 2, 3

[34] Zhou Wang, Alan C Bovik, Hamid R Sheikh, and Eero P Simoncelli. Image Quality Assessment: From Error Visibility to Structural Similarity. *IEEE Transactions on Image Processing*, 13(4):600–612, 2004. 7

[35] Yingyan Xu, Gaspard Zoss, Prashanth Chandran, Markus Gross, Derek Bradley, and Paulo Gotardo. ReNeRF: Relightable Neural Radiance Fields with Nearfield Lighting. In *Proceedings of the IEEE/CVF International Conference on Computer Vision*, pages 22581–22591, 2023. 5

[36] Yao Yao, Zixin Luo, Shiwei Li, Jingyang Zhang, Yufan Ren, Lei Zhou, Tian Fang, and Long Quan. BlendedMVS: A Large-Scale Dataset for Generalized Multi-View Stereo Networks. In *Proceedings of the IEEE/CVF Conference on Computer Vision and Pattern Recognition*, pages 1790–1799, 2020. 2

[37] Yao Yao, Jingyang Zhang, Jingbo Liu, Yihang Qu, Tian Fang, David McKinnon, Yanghai Tsin, and Long Quan. NeILF: Neural Incident Light Field for Physically-Based Material Estimation. In *European Conference on Computer Vision*, pages 700–716. Springer, 2022. 2

[38] Dongbin Zhang, Chuming Wang, Weitao Wang, Peihao Li, Minghan Qin, and Haoqian Wang. Gaussian in the Wild: 3D Gaussian Splatting for Unconstrained Image Collections. In *European Conference on Computer Vision*, pages 341–359. Springer, 2024. 2, 6, 8

[39] Richard Zhang, Phillip Isola, Alexei A Efros, Eli Shechtman, and Oliver Wang. The Unreasonable Effectiveness of Deep Features as a Perceptual Metric. In *Proceedings of the IEEE Conference on Computer Vision and Pattern Recognition*, pages 586–595, 2018. 7